Nanoscale Advances

ROYAL SOCIETY OF CHEMISTRY

PAPER

Cite this: *Nanoscale Adv.*, 2022, **4**, 5365

Construction of photo-induced zinc-doped carbon dots based on drug-resistant bactericides and their application for local treatment†

Zhuoling Zhong, ‡[a] Yaoyao Zhang,‡[b] Xiaoyun Fu,[c] Shuyao Liu, [a] Chuanwei Zhang,[a] Weijie Guo,[d] Xiaoping Xu*[a] and Liyun Liao*[e]

In this project, we propose a highly effective photosensitizer that breaks through drug-resistant bacterial infections with zinc-doped carbon dots. By passing through the membrane of drug-resistant bacteria, the photosensitizers produce ROS in bacteria under the action of blue light to directly kill bacteria, so as to realize the antibacterial local treatment of drug-resistant bacteria. The experiment firstly uses an efficient one-step hydrothermal method to prepare zinc-doped red-light CDs as photosensitizers, in which zinc metal was doped to improve the optical properties of the CDs. Then we try first to use EDTA as a second-step attenuator for preparing CDs to obtain photosensitizers with high-efficiency and low toxicity. *In vitro* cytotoxicity tests, bacterial effect tests, and *in vivo* animal experiments have also demonstrated that this antibacterial method has great potential for clinical translation, with a bactericidal efficiency of up to 90%. More notably, we used this antibacterial regimen seven times repeatedly to simulate the bacterial resistance process, with a bactericidal efficiency of up to 90% every time. The result indicated that *S. aureus* did not develop resistance to our method, showing that our method has the potential to break through drug-resistant bacterial infections as an alternative to antibiotic candidates.

Received 14th June 2022
Accepted 18th October 2022

DOI: 10.1039/d2na00375a

rsc.li/nanoscale-advances

Introduction

Drug-resistant bacteria seriously affect the lives and health of people around the world and are a hot topic of concern for researchers.[1] However, because of the widespread utility of antibiotics, a lot of bacteria have already developed resistance,[2,3] and researchers are urgently searching for a new non-resistant antibacterial solution or antimicrobial agent. Many physical antimicrobial options have received attention from scientists because of their low probability of resistance and low toxicity, such as radiation[4,5] and heat.[6,7] Among them, photodynamic therapy (PDT) is one of the means of treating cancer, especially skin cancer, and is a minimally invasive treatment method with the advantages of low drug resistance, less marginal tissue damage, and fewer toxic side effects than other traditional therapies such as surgery and radiotherapy.[8]

PDT consists of three elements: the photosensitizer, the excitation light, and the molecular oxygen in the tissue. The efficiency of reactive oxygen species (ROS) generation by photosensitizers and the unavailability of bacteria to develop drug resistance are two major factors determining the effectiveness of photodynamic therapy for the treatment of infections. Its basic principle[9,10] is shown in Scheme 1. Antimicrobial photodynamic therapy is based on the idea that a safe chemical compound, called a photosensitizer, should be activated by visible light with the appropriate wavelength to produce ROS which is toxic to pathogens. Generation of reactive oxygen species will take place along two alternative paths as soon as the photosensitizers are activated by light. The singlet active state 1PS* is formed after absorbing a photon with the ground-state photosensitizer. The active 1PS* state is short-lived and can undergo intersystem crossing to a long-lived triplet state, or alternatively could return to the ground state by fluorescence emission and heat. Usually the 3PS* acts as a mediator for type-I and type-II processes. Type-I: production of hydrogen peroxide (H_2O_2), hydroxyl radical ($HO^{\bullet}$), and superoxide anion ($^{\bullet}O_2^-$) by charge transfer from excited PS. Type-II: the 3PS* can undergo energy exchange immediately by triplet ground-state oxygen, resulting in the formation of singlet oxygen, $^1O_2$.[11]

[a]*Sichuan Research Center for Drug Precision Industrial Technology, West China School of Pharmacy, Sichuan University, Chengdu 610041, China. E-mail: zhongzhuoling@stu.scu.edu.cn; xuxp319@scu.edu.cn*

[b]*Department of Obstetrics and Gynecology, Key Laboratory of Birth Defects and Related of Women and Children of Ministry of Education, West China Second University Hospital, Sichuan University, Chengdu, Sichuan 610041, China*

[c]*Neijiang Medical School in Sichuan Province, Neijiang 641199, China*

[d]*West China School of Public Health, West China Fourth Hospital, Sichuan University, Chengdu 610041, China*

[e]*School of Pharmacy, Chengdu Medical College, 783, Xindu Avenue, Chengdu 610500, China. E-mail: llyhx210@tom.com*

† Electronic supplementary information (ESI) available. See DOI: https://doi.org/10.1039/d2na00375a

‡ These authors contributed equally to this work.

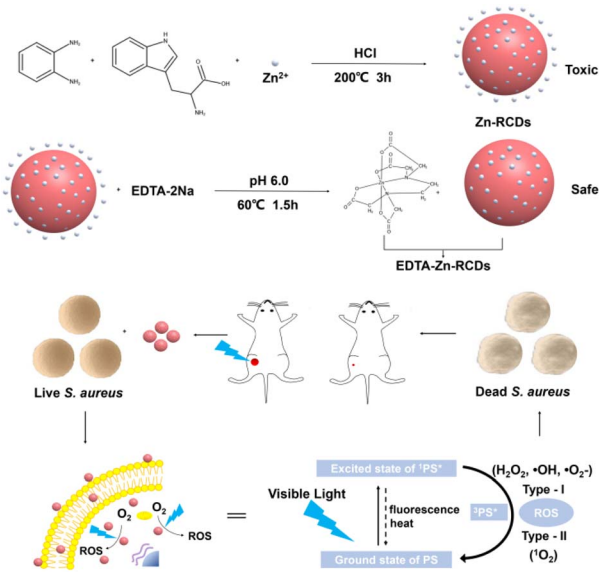

Scheme 1 Illustration of the fabrication process of EDTA–Zn-RCDs and the utilization of EDTA–Zn-RCDs as effective agents for synergistic bacteria killing.

However, common photosensitizers such as phthalocyanines, porphyrins, phenothiazines, and nano-semiconductor materials have disadvantages that limit their use. For example, although phthalocyanines have unique optical properties, they have obvious disadvantages such as poor water solubility and a tendency to aggregate. Porphyrins give a high yield of ROS but are often painful due to their strong photosensitivity.[12] Phenothiazines such as toluidine blue have been shown to have antibacterial properties, but are poorly targeted and have the same antibacterial properties when unirradiated, which is dark toxicity.[13] The diode photocatalyst, TiO_2, requires UV light for excitation, which occupies only 4% of the incident solar spectrum and is harmful to live organisms.[14] Although photosensitizers have shown good antibacterial activity in the above studies, they suffer from disadvantages such as causing pain, dark toxicity, lack of photocatalytic efficiency, and narrow excitation wavelengths, which severely limit their widespread use in photocatalysis.

Carbon dots were figured out in 2004 for the first time by Wang *et al.*[15] when they were preparing single-walled carbon nanotubes. They are of great interest to scholars because of their high biosafety, chemical stability, excellent optical properties, anti-photobleaching properties, low toxicity, and simple and diverse synthesis methods, and have a bright future in many fields such as antibacterial, biomarker, and biocatalytic applications.[16–18] They have provided different avenues for new antibacterial materials and photosensitizers. Ju *et al.*[19] prepared carbon dots using chloroform, diethylamine, and ammonium carbonate and found that the carbon dots were able to generate strong electrostatic interactions with bacteria thereby causing damage to the bacterial cell walls or cell membranes of *Staphylococcus aureus* and *Escherichia coli*. The nitrogen and zinc-doped luminescent carbon dots prepared by Das *et al.*[20] were able to kill *Escherichia coli* under light excitation. The carbon dot composite prepared by Meziani *et al.*[21] was found to be able to kill *E. coli* after 30 min of visible light irradiation. Although research on the use of carbon dots for photodynamic sterilization therapy is at an early stage, the exact mechanism is not yet fully understood. However, due to their unique fluorescence properties, stable chemistry, low toxicity, easy binding to bacteria and their biofilms, good light-induced electron transfer ability, and light absorption ability, they have the potential to become excellent photosensitizers and are of great importance for the development of new antibacterial therapies.

Many photo-catalytically active nanomaterials are currently used as photocatalysts for the study of electron transfer processes and charge separation.[22–25] The problem that this field encounters is developing lots of economical and high-efficiency photocatalysts to replace the existing ones based on expensive metal nanoparticles, like ruthenium nanoparticles.[26] Fortunately, CDs have special electron transfer and broadband light absorption capabilities and are abundant, cheap, and non-toxic.[27–38] These excellent properties facilitate intermolecular electron transfer, which are of paramount importance in lots of photo-oxidation interactions. To improve the electron transfer and photooxidation reactions of photocatalysts, the strategy of co-doping carbon dots with heteroatoms has attracted the attention of scholars and has wide applications in biomolecular labeling, chemical sensing, optoelectronics, and trace element detection.[39–42] In recent years, there have been fewer reports on the doping of metal atoms, among which Wu *et al.*[43] reported the co-doping of CDs with nitrogen and copper to enhance their electron-giving and accepting abilities. However, there is some increase in toxicity when doped metal atoms enter the CD matrix. Whereas zinc is an important element that assists many electron transfer processes, it is a trace element in various biological systems as well with negligible toxicity and zinc deficiency can lead to a lot of health problems. So doping the CD matrix with zinc may be beneficial to improve the performance of nanomaterials,[44] and there are also examples in the literature to demonstrate that the properties of photodetectors will be significantly enhanced by intervention with ZnO quantum dot/carbon nanodot hybrid films, as reported by Guo *et al.*[45] The preparation of ZnO/carbon quantum dots, which have outstanding photocatalytic properties, by the sol–gel method was reported by Zhang *et al.*[46] The preparation of ZnO-doped CDs with QYs of 29.3% chitosan/ion complex was reported by Li *et al.*[47]

Therefore, we propose a highly effective photosensitizer that breaks through drug-resistant bacterial infections with the aid of zinc-doped carbon dots. By passing through the membrane of drug-resistant bacteria, the photosensitizer produces ROS in bacteria under the action of blue light power to directly kill the bacteria, so as to realize the antibacterial local treatment of drug-resistant bacteria and their traumatic infection model. At the same time, how to use visible light, a resourceful, economical, and environmentally friendly energy source, and convert it into chemical energy or other forms has attracted the interest of researchers in recent years. In this project, blue light, which has higher energy, and is safer, lower in cost, and easier

to obtain among all visible lights, was chosen as the excitation light, and blue light has been reported to excite photosensitizers to produce ROS,[48] which has a certain inhibition effect on brain glioma cells. A highly efficient and economical one-step hydrothermal approach was used to construct zinc-doped red light carbon dots as a photosensitizer. And zinc metal was used as a photocatalyst for the photodynamic reaction, which greatly improved the efficiency of ROS generation and the bactericidal rate, which is higher than that of PpIX. To reduce the cytotoxicity caused by free metal zinc ions under acidic reaction conditions, the first attempt was made to employ EDTA as a second-step attenuator in preparing CDs to obtain photosensitizers with high efficiency and low toxicity. And this is a novel way for the construction of highly efficient and low-toxicity metal-doped carbon dots. The bactericidal efficiency was 90% after seven repeated treatments in the simulated bacterial resistance process, indicating that *S. aureus* did not develop resistance to our method. The results showed that our method has the potential to break through drug-resistant bacterial infections as an alternative to antibiotic treatment candidates as well as one of the candidate treatment regimens. And with this antimicrobial solution, firstly, the researcher can visually locate the lesion or direct the light at the lesion by imaging. Secondly, as the photosensitizer accumulates in one infected area, the inflamed area is concretely targeted as soon as the light reaches the inflamed area. In subsequent studies in mouse wound models, the antimicrobial effect is good, requiring only one complete treatment to show a significant difference with a bactericidal efficiency of 91.17%. The method provides a novel antimicrobial alternative to antibiotics for subsequent studies for antimicrobial treatment in deeper tissues and organs. The process of preparing EDTA–Zn-RCDs and the bactericidal principle are shown in Scheme 1.

Experimental

Instruments, reagents, and materials

Fluorescence spectrophotometer RF6000 (Shimadzu), microplate reader Varioskan LMX (Thermo), UV-2300 UV-visible spectrophotometer (Shanghai Tianmei Scientific Instruments Co., Ltd), infrared spectrometer (Invenio R, Bruker), Sartorius BT 125D 1-in-100,000 electronic balance (Germany) SHANGPING PA 2004 one-millionth electronic balance (Shanghai Tianping Instrument Factory), KL 10260D ultrasonic cleaner (Shanghai Jinghe Analytical Instruments Co., Ltd), water purifier (Chengdu Pincheng Technology Co., Ltd), transmission electron microscope (H-600, Hitachi, Japan), scanning electron microscope (S-3400, Hitachi, Japan), fluorescence microscope (Olympus, Japan), Pannoramic MIDI pathology section scanner, biological safety cabinet (Sojung-Antai), X-ray photoelectron spectroscopy instrument (XPS, PHI-5000versaprobe), blue light (Qixin, 450–460 nm, 30 μW cm^{-2}).

Ethanol (analytical purity, Chengdu Hi-Tech Shiyang Chemical Preparation Plant), *o*-phenylenediamine (99%, Shanghai Aladdin Biochemical Technology Co., Ltd), L-tryptophan (99%, Shanghai Maclean Biotechnology Co., Ltd), hydrochloric acid (analytical purity, Xilong Science Co., Ltd), disodium ethylenediaminetetraacetate (EDTA-2Na, analytical purity, Fuchen Chemical Reagent Co., Ltd), zinc chloride (analytical purity), sodium hydroxide (analytical purity), agar powder (Chengdu Kolon Chemical Co., Ltd), yeast leaching powder (Chengdu Kolon Chemical Co., Ltd), tryptone (Beijing Auboxing Biotechnology Co., Ltd), anhydrous ether (analytical purity, Xilong Science Co., Ltd). Trypsin, DMEM, and FBS were all imported reagents. Glutaraldehyde fixative (2.5%) was purchased from Shanghai Yuanye Biotechnology Co. The reactive oxygen assay kit (DCFDA, Solarbio) and propidium iodide (PI) were purchased from Shanghai Biyuntian Biotechnology Co., singlet oxygen sensor green reagent was from SOSG, Meilunbio, and protoporphyrin IX (PpIX) from Sigma.

Mice (BALB/c, 7 weeks, female, SPF, Beijing Huafukang Biotechnology Co., Ltd). L929 cells, *Staphylococcus aureus*, and *Escherichia coli* were provided by the State Key Laboratory of Sichuan University.

Preparation of RCDs, Zn-RCDs, and EDTA–Zn-RCDs

RCDs. Based on the literature,[49] we selected red carbon dots (RCDs), which are simple to prepare, rapid to synthesize, and stable for *in vivo* local studies. The RCDs were prepared by making use of a one-step hydrothermal approach: 108 mg of *o*-phenylenediamine and 54 mg of L-tryptophan were weighed in a clean reactor with 10 ml of deionized water. 200 μl of concentrated hydrochloric acid was added and mixed well, and the experiment was conducted at 200 °C for 3 hours. The resulting mixture was sterilized using a 0.22 μm filter membrane and then lyophilized to obtain the carbon dots powder and set aside.

Zn-RCDs. To improve the photocatalytic efficiency of RCDs as photosensitizers, we doped zinc into the carbon sites to enhance their bactericidal effect. The Zn-RCDs were also prepared by making use of a one-step hydrothermal approach: 108 mg of *o*-phenylenediamine, 54 mg of L-tryptophan, and 136 mg of zinc chloride were weighed in a clean reactor containing 10 ml of deionized water. 200 μl of concentrated hydrochloric acid was added and mixed well, and the experiment was performed at 200 °C for 3 hours. The resulting mixture was decontaminated using a 0.22 μm filter membrane and then lyophilized to obtain carbon dots powder.

EDTA–Zn-RCDs. As Zn-RCDs are highly bactericidal but cytotoxic, subsequent experiments have shown that the cause of cytotoxicity is the free zinc ions under acidic reaction conditions. Because EDTA contains 6 coordination atoms and has strong coordination ability, it is often used as a metal ion detoxification agent. For the first time, we applied EDTA as a second-step detoxification agent in the preparation of CDs to produce highly efficient and low-toxicity EDTA–Zn-RCDs: 108 mg of *o*-phenylenediamine, 54 mg of L-tryptophan and 136 mg of zinc chloride were weighed into a clean reactor with 10 ml of deionized water. 200 μl of concentrated hydrochloric acid was added and mixed well, and the experiment was conducted at 200 °C for 3 hours. 372.24 mg of EDTA-2Na was added to the liquid mixture, mixed well, the pH was adjusted to 6.0 and the reaction was conducted in a water bath at 60 °C for 1.5

hours. Then this mixture was decontaminated using a 0.22 μm filter membrane and then lyophilized to obtain carbon dots powder and set aside.

EDTA–Zn. 136 mg of zinc chloride and 372.24 mg of EDTA-2Na were weighed into the liquid mixture, mixed well, the pH was adjusted to 6.0 and the reaction was conducted in a water bath at 60 °C for 1.5 hours. Then this mixture was decontaminated with a 0.22 μm filter membrane and then lyophilized to obtain a powder and set aside.

Characterization of RCDs, Zn-RCDs, and EDTA–Zn-RCDs

5 mg lyophilized powder was added to 5 ml PBS solution and 1 mg ml^{-1} RCD, Zn-RCD, and EDTA–Zn-RCD solutions were prepared by dropping the respective powder on a copper mesh, and then they were left to dry naturally, and then the morphology and size of the CDs were observed using a transmission electron microscope (TEM). EDTA–Zn-RCDs with the largest particle size were observed in a dark field and scanned for Zn. 20 mg freeze-dried RCD, Zn-RCD, and EDTA–Zn-RCD powders were mixed with potassium bromide in a suitable ratio and pressed into sheets. The FTIR spectra of RCDs, Zn-RCDs, and EDTA–Zn-RCDs were recorded using an infrared spectrometer. 5 mg lyophilized powder was added to 5 ml PBS solution and 1 mg ml^{-1} RCD, Zn-RCD and EDTA–Zn-RCD solutions were prepared. Then the UV-Vis absorption spectra of carbon dots were recorded on a UV-Vis spectrophotometer. 5 mg lyophilized powder was added to 5 ml PBS solution and 1 mg ml^{-1} RCD, Zn-RCD and EDTA–Zn-RCD solutions were prepared. Their fluorescence spectra were recorded on a fluorescence spectrophotometer. 20 mg lyophilized RCD, Zn-RCD, and EDTA–Zn-RCD powders were taken and sent to the analysis and testing center for inspection. They were kept away from light and vacuum, XPS experiments were conducted by professional teachers.

Cell culture as well as biocompatibility assays

Cytotoxicity assays for RCDs, Zn-RCDs, *o*-phenylenediamine, Zn^{2+}, EDTA–Zn-RCDs, and EDTA–Zn were performed using the CCK8 method. L929 cells were resuscitated in an H-DMEM medium with 1% double antibodies and 10% fetal bovine serum and then cultured in a cell culture incubator. L929 cells in the logarithmic growth phase were inoculated in 96-well plates with 5000 cells per well and incubated at 37 °C in a 5% CO_2 cell culture incubator. 24 hours later, the cells were transferred into new concentrations of RCD, Zn-RCD, *o*-phenylenediamine, Zn^{2+}, EDTA–Zn-RCD and EDTA–Zn culture solutions (5, 10, 25, 50, 100, 200, 400 and 600 μg ml^{-1}), with 6 replicate wells set up for each concentration. The wells were washed 3 times with PBS. 100 μl of culture medium containing CCK-8 10 μl was added and incubated for 2 hours. The optical density values of the wells were measured at 450 nm on a microplate reader. The optical density value was used to express the concentration of each group and to calculate the relative survival rate of L929 cells (%) = (OD values of experimental group/OD values of the blank control group) × 100%.

Bacterial culture and bactericidal effect experiments

The experiment was divided into 2 groups: carbon dots + blue light group and blank control group. Firstly, an *S. aureus* colony or an *E. coli* colony was taken on a plate with a sterilized ring and inoculated in LB culture solution. After 18–24 h incubation, 100 μl of the bacterial solution was taken and placed at 600 nm to determine the optical density value, OD600 = 0.5. The corresponding strain concentration was 10^8 CFU ml^{-1}, diluted at 1 : 100 and ready to be used. The bacteria in the logarithmic growth phase were inoculated to 96-well plates at 100 μl per well. For the carbon dots + blue light group, different final concentrations of RCD, Zn-RCD, *o*-phenylenediamine, Zn ions, EDTA–Zn-RCD and EDTA–Zn solution (5, 10, 25, 50, 100, 200, 400 and 600 μg ml^{-1}) were added, prepared using PBS solution before, shaken well, incubated at 37 °C for 15 minutes, and irradiated with blue light for 30 minutes. The distance between the blue light and the sample was 20 cm and the sample was incubated at 37 °C for 24 h, protected from light. At the same time, the group without the addition of drugs and blue light irradiation was set up as a blank control group, and the optical density value was measured at a wavelength of 600 nm. The optical density value was used to express the concentration of each group and to calculate the relative survival rate of bacteria (%) = (OD value of experimental group/OD value of blank control group) × 100%.

Quantitative test of $^1O_2$ *in vitro*

The generation of extracellular singlet oxygen was measured by the green fluorescence emitted by SOSG. The cell-free LB culture medium was inoculated with 100 μl per well to 96 well plates. The final concentration of 600 μg /ml^{-1} of RCD, Zn-RCD, EDTA–Zn-RCD, and PpIX solution, prepared with PBS solution before, was added, 6 multiple wells were set, shaken well, and then irradiated with blue light for 30 min. The distance between the blue light lamp and the sample was 20 cm. The same amount of PBS group was set as the blank control group. After the illumination, SOSG staining is added immediately to obtain the final concentration of 5 μM. The solution was shaken well, incubated at 37 °C for 15 min and kept away from light. Then, the fluorescence intensity of SOSG in each group was measured with a microplate reader, setting the excitation wavelength of 504 nm and emission wavelength of 525 nm.

Quantitative test of ROS

The production of ROS in bacterial cells was measured from the green fluorescence emitted by DCFDA. The bacterial suspension was stained with 10 μM DCFDA at 37 °C for 20 minutes, mixed once every 5 minutes, and then washed three times with PBS. The washed cells were inoculated into 96 well plates with 100 μl per well. The final concentration of 600 μg ml^{-1} of RCDs, Zn-RCDs, EDTA–Zn-RCDs, and PpIX, prepared with PBS solution before, was added, 6 multiple wells were set, shaken well, and incubated at 37 °C for 15 min; light was avoided, and then irradiated with blue light for 30 min. The distance between the blue light lamp and the sample was 20 cm. The same amount of

PBS group was added as the blank control group. Then, the fluorescence intensity of DCFDA in each group was measured using an enzyme labeling instrument, setting the excitation wavelength of 485 nm and emission wavelength of 525 nm.

Validation experiment of the bactericidal mechanism and the ROS staining assay

Validation experiment of the bactericidal mechanism. The green fluorescence emitted by DCFDA was used to determine the production of ROS in bacterial cells. Bacterial suspensions were stained with 10 μM DCFDA for 20 minutes at 37 °C in the dark, mixed every 5 min, and washed three times with PBS. The washed cells were inoculated into 96-well plates at 100 μl per well, and different final concentrations of EDTA–Zn-RCD solution (5, 10, 25, 50, 100, 200, 400, and 600 μg ml^{-1}), prepared using PBS solution before, were added, shaken well, incubated for 15 minutes at 37 °C, and then irradiated with blue light for 30 minutes. The distance between the blue light lamp and the sample was 20 cm, while the group without the addition of drugs and no blue light irradiation was set up as a blank control group, followed by the use of the microplate reader and tuning parameters such as the excitation wavelength at 488 nm and emission wavelength at 525 nm. The fluorescence intensity of DCFDA was measured for different concentrations of the EDTA–Zn-RCD group.

The ROS staining experiment. The ROS staining experiment was divided into 4 groups: carbon dots + blue light group, carbon dots group, blue light group, and blank control group to determine the production of ROS in bacterial cells using the green fluorescence emitted by DCFDA. Bacterial suspensions were stained with 10 μM DCFDA for 20 minutes at 37 °C in the dark, mixed every 5 minutes, then centrifuged at 4000 rpm and washed three times with PBS. The carbon dots + blue light group incubated the washed cells with a final concentration of 600 μg ml^{-1} EDTA–Zn-RCDs, prepared using PBS solution before, for 15 minutes at 37 °C and blue light for 30 minutes, with a distance of 20 cm between the blue light and the sample. The carbon dot group incubated the washed cells with a final concentration of 600 μg ml^{-1} EDTA–Zn-RCDs, prepared using PBS solution before, at 37 °C for 15 min then incubated for 30 min protected from light. The blue light group incubated the washed cells for 15 minutes at 37 °C and then the cells were incubated again with blue light for 30 min. The blank control group incubated the washed cells for 15 min at 37 °C and then incubated them for 30 min protected from light, followed by observation of green fluorescent ROS-producing bacterial cells at 485 nm excitation wavelength using a fluorescence microscope. The observation areas were photographed randomly (3 areas per sample).

Live and dead bacteria staining experiments

The live and dead cell staining experiment was divided into 4 groups: carbon dots + blue light group, carbon dot group, blue light group, and blank control group, using PI to stain the dead cells with red fluorescence. The carbon dot + blue light group incubated the washed cells with a final concentration of 600 μg ml^{-1} EDTA–Zn-RCDs, prepared with PBS solution before, for 15 minutes at 37 °C and the cells were incubated with blue light for 30 minutes, with a distance of 20 cm between the blue light lamp and the sample. The carbon dot group incubated the washed cells with a final concentration of 600 μg ml^{-1} EDTA–Zn-RCDs, prepared using PBS solution before, at 37 °C for 15 min then the cells were incubated for 30 min protected from light. The blue light group incubated the washed cells at 37 °C for 15 min then the cells were irradiated with blue light for 30 min. The blank control group incubated the washed cells at 37 °C for 15 min then incubated them for 30 min protected from light. All 4 groups were incubated for 24 h at 37 °C, centrifuged at 4000 rpm, washed three times with PBS, stained with 4 μM PI for 30 min at 37 °C in the dark, mixed every 5 min, then centrifuged, washed three times with PBS and resuspended with PBS. Bacterial cells producing red fluorescence were then observed using a fluorescence microscope at 535 nm excitation wavelength. The observation areas were photographed randomly (3 areas per sample).

Bacterial plate assay

The standard plate count method is a method commonly used to assess the number of viable cells in bacterial suspensions at low cell concentrations (approximately 10^3 cells per ml) and is used to demonstrate the antibacterial effect of EDTA–Zn-RCDs + blue light radiation. The experiment was divided into 4 groups: carbon dot + blue light group, carbon dot group, blue light group and blank control, with LB culture medium appropriately diluted in the logarithmic growth phase for 10^3 units per ml. In the carbon dot + blue light group, the diluted cells were incubated with a final concentration of 600 μg ml^{-1} EDTA–Zn-RCDs, prepared with PBS solution before, at 37 °C for 15 min and blue light for 30 min, with a distance of 20 cm between the blue light and the sample. The carbon dot group incubated the diluted cells with a final concentration of 600 μg ml^{-1} EDTA–Zn-RCDs, prepared with PBS solution before, at 37 °C for 15 min then incubated for 30 min protected from light. The blue light group incubated the diluted cells at 37 °C for 15 min then the cells were irradiated with blue light for 30 min. The blank control group incubated the diluted cells at 37 °C for 15 min then incubated them for 30 min protected from light. The blue light group incubated the diluted cells at 37 °C for 15 min then incubated them for 30 min protected from light. Then, four groups of bacteria were spread onto LB agar plates using spreaders, and the plates were incubated at 37 °C for 24 hours. The number of colony forming units was visually inspected.

Drug resistance assay

The experiment was divided into 2 groups: carbon dot + blue light group and blank control group. Firstly, an *S. aureus* colony was taken from the plate with a sterilized ring and inoculated in LB culture solution. After 18–24 h incubation, 100 μl of the bacterial solution was taken at 600 nm wavelength to determine the optical density value: OD600 = 0.5; the corresponding strain concentration was 10^8 CFU ml^{-1}, dilution at 1 : 100 is to be used. Took the logarithmic growth period of *S. aureus* to 100 μl

per well inoculated into 96-well plate. Carbon dot + blue light group: added final concentration 600 μg ml^{-1} EDTA–Zn-RCDs solution, prepared by PBS solution before, set up 6 replicate wells, shake well, incubated at 37 °C for 15 min, then blue light irradiation for 30 min, the distance between the blue light lamp and the sample was 20 cm, incubate at 37 °C and avoid light for 24 h. At the same time, the group with no drug added and no blue light irradiation was set up as a blank control group, and the optical density value was measured at a wavelength of 600 nm. The optical density value was used to express the concentration of each group and to calculate the relative survival rate of bacteria (%) = (OD value of the experimental group/OD value of the blank control group) × 100%. The surviving bacterial cells were re-cultured in a fresh LB medium for 24 hours. The 7 treatment rounds mentioned above were then performed and the relative bacterial survival rate was calculated for each round separately.

In vivo antimicrobial assay

A total of 30 mice were divided into five groups: the healthy group was called the no-modeling group; the modeling group was divided into four groups: the PBS group, the blue light irradiation group alone, the EDTA–Zn-RCDs alone group, and the EDTA–Zn-RCDs + blue light irradiation group, with six mice in each group. Firstly, a mouse skin wound model with bacterial infection was established. In the first step, mice were treated with ether for anesthesia. Then, a circular impression of 1 cm in diameter was made on the dorsal debridement area, and the skin was cut along the edge, followed by the injection of 100 μl of prepared *S. aureus* solution at a concentration of 10^8 CFU ml^{-1} at the circumference of the wound. The next day a fluid discharge with redness and swelling was visible on the dorsal wound surface of the mice, indicating a successful model. Subsequently, the infected mice were randomly divided into 4 groups of 6 mice each. The 4 groups of mice received different treatment regimens: PBS, EDTA–Zn-RCDs (600 μg ml^{-1}), prepared with PBS solution before, blue light irradiation and EDTA–Zn-RCDs (600 μg ml^{-1}) + blue light irradiation. 100 μl of EDTA–Zn-RCDs (600 μg ml^{-1}) and PBS were added dropwise to the infected wounds, wherein the light irradiation group was irradiated with blue light for 30 min, with a distance of 20 cm between the blue light and the sample. During the treatment, the mice were under anesthesia. Wound pictures were collected at different time points (0 d, 2 d, 4 d, 6 d, 8 d, and 10 d). After 10 d, first, the wound was sampled for bacteria and the lesioned skin of the posterior back was taken and homogenized at a ratio of 10 ml of sterile saline per 50 mg of skin. The homogenate was used as the stock solution and diluted to 10^{-1}, 10^{-2}, 10^{-3} and 10^{-4} in order, and 100 μl of dilutions were taken in LB plates, and 3 plates were set up for each dilution. Tissues from the skin of mouse wounds and internal organs (heart, liver, spleen, lung, and kidney) were collected for histological analysis (hematoxylin and eosin staining: H&E).

All animal procedures were performed following the Guidelines for Care and Use of Laboratory Animals of Sichuan University and approved by the Animal Ethics Committee of Sichuan University (110322210101152132).[50]

Stability experiment

Stability experiment of EDTA–Zn and EDTA–Zn-RCD lyophilized powders. We conducted an L929 cytotoxicity test on the same batch of EDTA–Zn and EDTA–Zn-RCD powder every 4 days within 28 days to investigate the stability of EDTA–Zn and EDTA–Zn-RCD lyophilized powder. The concentrations of EDTA–Zn and EDTA–Zn-RCDs were 600 μg ml^{-1}.

Photostability experiment of EDTA–Zn-RCD solution. The effects of salt ion concentration, pH value, UV radiation time and storage time on the fluorescence intensity of 600 μg ml^{-1} EDTA–Zn-RCD solution were determined.

Statistical analysis. Data were expressed as mean ± standard deviation. The statistical significance of differences between treatments was assessed using the one-way ANOVA test.

Results and discussion

Characterization of RCDs, Zn-RCDs, and EDTA–Zn-RCDs

According to Fig. S1(a) and (b),† RCDs are monodisperse spherical particles as observed by TEM, and the particle size is about 16 nm, which is relatively uniform. According to Fig. S1(c) and (d),† Zn-RCDs are monodisperse spherical particles with the size of about 25 nm according to TEM images. Particles with darker color and smaller sizes can be observed on their surface, which are speculated to be zinc atoms doped on the surface of carbon dots. The particle size is larger than that of RCDs, which indicates that RCDs were successfully doped with Zn. According to Fig. S1(e) and (f)† which is the same as Fig. 1(a) and (b), EDTA–Zn-RCDs are monodisperse spherical particles with a size of about 25 nm according to TEM images as well. They are very similar to the morphology shown in Fig. S1(c) and (d)† of Zn-RCDs, which shows that EDTA binds to the free zinc ions rather than the zinc ions doped on the surface of RCDs. Smaller particles of darker color can be observed on the surface, presumably as zinc atoms were doped on the surface of the CDs. Meanwhile, the scanning results of the corresponding TEM elemental mappings show that Zn element is evenly distributed in the same particles, as depicted in Fig. 1(c) and (d), which

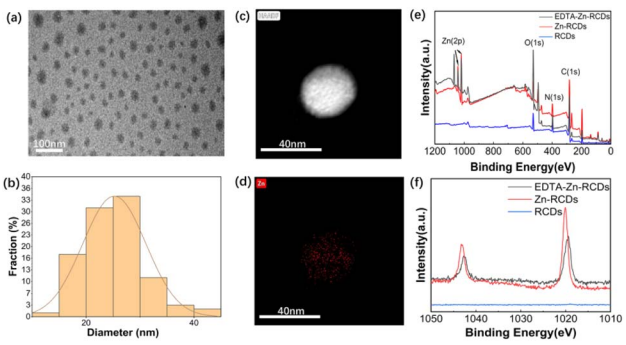

Fig. 1 (a) TEM for EDTA–Zn-RCDs; (b) particle size distributions of EDTA–Zn-RCDs determined by the DLS method; (c) dark-field TEM image of EDTA–Zn-RCDs, and (d) corresponding TEM elemental mappings of the Zn edge signal. (e) The total elemental analysis XPS spectra of RCDs, Zn-RCDs and EDTA–Zn-RCDs; (f) the divided peak of Zn2p XPS spectra of RCDs, Zn-RCDs and EDTA–Zn-RCDs.

proves once again that zinc ions are successfully doped. EDTA–Zn-RCDs are in a liquid state when they are taken out from the reactor. To prolong the storage time, we usually freeze-dry the carbon dots to convert them from a liquid to a powder. When we conduct TEM experiments, we usually re-dissolve the powder in PBS and the cluster substances can be observed by TEM. However, cluster substances cannot be observed by TEM, when the raw solution is taken out from the reactor without freeze-drying. It is speculated that cluster substances are produced in the process of freeze-drying and re-dissolution. Because the lyophilized sample contains cluster substances, to avoid causing vascular thrombosis, local administration is selected for subsequent *in vivo* experiments. If interested, systemic administration can be explored based on stock solutions.

XPS characterization in Fig. 1(e) and (f) shows that EDTA–Zn-RCDs and Zn-RCDs contain Zn element and the partial peaks of Zn2p Fig. 1(f) show two strong absorptions at 1020 and 1043 eV, indicating the existence of Zn, and it can be seen from the figure that Zn element in EDTA–Zn-RCDs and Zn-RCDs accounts for a higher proportion than N and C elements, which once again proves the successful doping of zinc ions.

According to Fig. S2(a),† RCDs have six peaks at 228 nm, 241 nm, 260 nm, 270 nm, 280 nm, and 450 nm, of which the absorption peak at 280 nm is attributed to the π–π* transition of the C=C bond, and the absorption peak at 450 nm may be due to the n–π* transition. According to Fig. S2(b),† there are 11 peaks of Zn-RCDs at 218 nm, 233 nm, 248 nm, 262 nm, 270 nm, 286 nm, 380 nm, 400 nm, 460 nm, 552 nm, and 600 nm, which prove that RCDs are successfully doped with Zn, resulting in great changes in the peak shape of Zn-RCDs. Zn-RCDs have more absorption peaks in the visible region than RCDs, even at 610 nm. It is proved that the optical performance of CDs doped with zinc metal is improved and the CDs can make better use of visible light which is rich in natural resources. According to Fig. S2(c),† EDTA–Zn-RCDs have seven absorption peaks at 219 nm, 232 nm, 248 nm, 261 nm, 272 nm, 280 nm, and 415 nm, of which the absorption peak at 280 nm is attributed to the π–π* transition of the C=C bond, and the absorption at 415 nm may be due to the n–π* transition. EDTA–Zn-RCDs is obtained by the complexation reaction between Zn-RCDs and EDTA. The change of peak shape compared with Zn-RCDs proves the success of the complexation reaction. And the three CDs had a wider wavelength absorption at 400–500 nm, while the wavelength range of blue light was 400–450 nm just within this range, which provided some theoretical basis for EDTA–Zn-RCDs using the energy of blue light to generate ROS.

According to Fig. S3(a),† the absorption peak of RCDs is centered at 3386.27 cm^{-1} which is attributed to the O–H and N–H stretching vibration; the peak of 1060.09 cm^{-1} may reflect the stretching vibration of C–N, and the absorption peak at 1457.08 cm^{-1} corresponds to the bending vibration of C–O. According to Fig. S3(b),† the absorption peak of Zn-RCDs is centered at 3390.56 cm^{-1} which is attributed to the O–H and N–H stretching vibration, and the peak of 1085.84 cm^{-1} may reflect the stretching vibration of C–N. It proves that RCDs were successfully doped with Zn, resulting in great changes in the peak shape of Zn-RCDs. From Fig. S3(c),† the absorption peak of EDTA–Zn-RCDs is centered at 3369.78 cm^{-1} which is attributed to the telescopic vibrations of O–H and N–H. The peak at 1106.23 cm^{-1} may reflect the stretching vibration of C–N, and the absorption peak at 1581.62 cm^{-1} corresponds to the in-plane bending vibration of N–H. The change of peak shape of EDTA–Zn-RCDs compared with Zn-RCDs proves the success of the complexation reaction. The above analysis indicates that these three constructed CDs mostly contain carbon, oxygen, and nitrogen elements.

In Fig. S4(a),† RCDs display bicentric excitation and emission. First, the excitation wavelength increases from 260 nm to 305 nm. The fluorescence intensity of RCDs increases with the increase of excitation wavelength in the range of 260–295 nm. In the range of 295–305 nm, the fluorescence intensity decreases with the increase of excitation wavelength, indicating that the maximum excitation wavelength of the first center in RCDs is 295 nm. There are two maximum emission wavelengths, at 342 nm and 700 nm, and the fluorescence performance is good. Then, the excitation wavelength increases from 580 nm to 620 nm, and the fluorescence intensity of RCDs increases with the increase of excitation wavelength in the range of 580–600 nm. In the wavelength range of 600–620 nm, the fluorescence intensity decreases with the increase of excitation wavelength, indicating that the maximum excitation wavelength of the second center in RCDs is 600 nm, while the maximum emission wavelength is 612 nm. According to Fig. S4(b),† Zn-RCDs show bicentric excitation and emission. Firstly, the excitation wavelength increases from 240 nm to 310 nm. The fluorescence intensity of Zn-RCDs increases with the increase of excitation wavelength in the range of 240–300 nm. In the wavelength range of 300–310 nm, the fluorescence intensity decreases with the increase of excitation wavelength, indicating that the maximum excitation wavelength of the first center of Zn-RCDs is 300 nm. There are two maximum emission wavelengths, 344 nm, and 702 nm, respectively. Then the excitation wavelength increases from 540 nm to 620 nm, and the fluorescence intensity of Zn-RCDs increases with the increase of excitation wavelength in the range of 540–610 nm. In the wavelength range of 610–620 nm, the fluorescence intensity decreases with the increase of excitation wavelength, indicating that the maximum excitation wavelength of the second center of Zn-RCDs is 610 nm, while the maximum emission wavelength is 615 nm, and the fluorescence performance is good. The emission peak of Zn-RCDs is slightly red-shifted compared with RCDs, and the emission intensity at 615 nm is significantly improved. It is proved that the optical properties of CDs doped with zinc metal are improved. From Fig. S4(c),† EDTA–Zn-RCDs exhibit single-center excitation and emission. The excitation wavelength increased from 240 nm to 300 nm, and the fluorescence intensity of EDTA–Zn-RCDs increased with increasing excitation wavelength in the wavelength range of 240–260 nm, and decreased with increasing excitation wavelength in the wavelength range of 260–300 nm, indicating that the maximum excitation wavelength of EDTA–Zn-RCDs was 260 nm, while there were two maximum emission wavelengths, 345 nm and 703 nm respectively, with good fluorescence performance. Compared with Zn-RCDs, the emission light of EDTA–Zn-RCDs

disappears at about 610 nm, which can also prove the success of the EDTA complexation reaction.

Cellular biocompatibility assay and bactericidal effect assay

We further illustrated the nature of EDTA–Zn-RCDs by cellular experiments, as depicted in Fig. 2(a) and 3(a). The cytotoxicity of RCDs reached the threshold at a concentration of 200 μg ml^{-1}, and the average survival rate of bacteria was 57.85% and the average bactericidal rate was 42.15%. We wished to improve the bactericidal efficiency of the drug by doping the carbon dots with Zn metal, which can help the carbon dot to improve the photo-oxidative catalytic efficiency of the surface. These results are shown in Fig. 2(b) and 3(b), where the cytotoxicity of Zn-RCDs reached the threshold at a concentration of 25 μg ml^{-1}, corresponding to an average survival rate of 59.3% and an average bactericidal rate of 40.7% for bacteria, while the concentration of Zn-RCDs reached 200 μg ml^{-1}, corresponding to an average survival rate of 11.8% and an average bactericidal rate of 88.2%. We attempted to reduce the cytotoxicity of Zn-RCDs while maintaining their good bactericidal effect and investigated the cytotoxicity and bactericidal performance of Zn-RCDs for two substances, *o*-phenylenediamine and free zinc ions, which may produce toxicity in the preparation process. As depicted in Fig. 2(c) and 3(c), the cell survival rate was still above 75% at concentrations of 0–600 μg ml^{-1} of *o*-phenylenediamine, and the average survival rate of bacteria was greater than 98.7%, indicating that the toxicity of *o*-phenylenediamine was minimal and that it had no bactericidal effect as well as photocatalytic oxidation activity. In contrast, when the properties of free zinc ions were examined alone, as depicted in Fig. 2(d) and 3(d), 5 μg ml^{-1} of zinc ions produced a significant toxic effect on L929 cells, while the average bacterial survival rate for 600 μg ml^{-1} of zinc ions was 43.38% and the average bactericidal rate was 56.62%. The inhibitory effect of free zinc ions on bacteria was observed to be associated with toxicity, with no inhibition with increasing light time. We speculate that free Zn ions lead to high cytotoxicity and it is imperative to select a method that reduces the toxicity of Zn ions while maintaining the good bactericidal effect of Zn-RCDs.

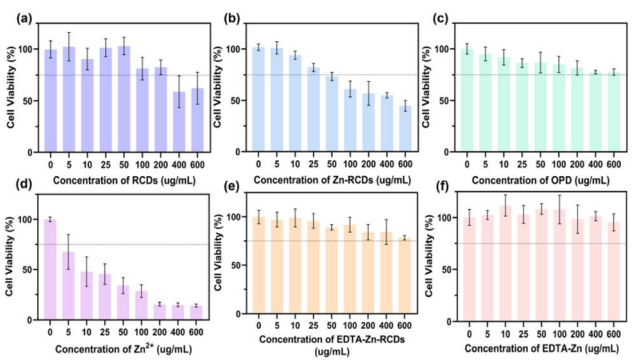

Fig. 2 Results of the cytotoxic test: (a) the influence of RCDs on L929 cells; (b) the influence of Zn-RCDs on L929 cells; (c) the influence of OPD on L929 cells; (d) the effect of Zn^{2+} on L929 cells; (e) the influence of EDTA–Zn-RCDs on L929 cells; (f) the influence of EDTA–Zn on L929 cells. ($n = 6$.)

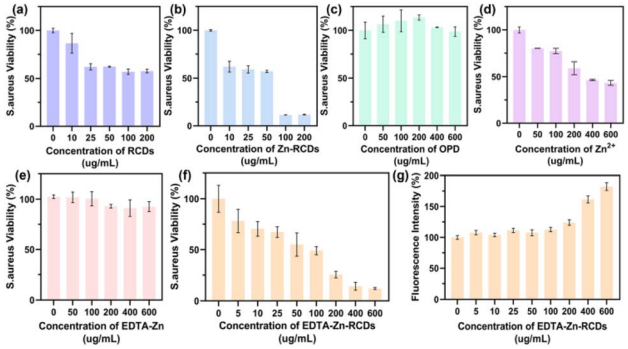

Fig. 3 The viability of *S. aureus* cells incubated with different concentrations of substances (incubation time 15 min) was determined at 24 h after irradiation. (a) The influence of RCDs on *S. aureus* cells; (b) the influence of Zn-RCDs on *S. aureus* cells; (c) the influence of OPD on *S. aureus* cells; (d) the influence of Zn^{2+} on *S. aureus* cells; (e) the influence of EDTA–Zn on *S. aureus* cells; (f) the influence of EDTA–Zn-RCDs on *S. aureus* cells; (g) intracellular ROS generation by *S. aureus* treated with EDTA–Zn-RCDs was probed by DCFDA immediately after irradiation. ($n = 6$.)

Due to its special structure, EDTA has excellent coordination ability and is mostly used as a heavy metal complexing agent for a wide range of applications. We attempted the reaction of EDTA with free zinc ions in Zn-RCDs to reduce their toxicity, and then examined the nature of the products, as depicted in Fig. 2(e) and 3(f), where the concentrations of EDTA–Zn-RCDs were in the range of 0–600 μg ml^{-1}. The L929 cell survival remained above 75%, and the average survival rate of bacteria showed a decreasing trend as the concentration of EDTA–Zn-RCDs increased and reached 11.9% and 88.1% average bactericidal rate when their concentration reached 600 μg ml^{-1}. Meanwhile, we investigated the properties of EDTA–Zn, a simple complexation product of Zn ion and EDTA without the participation of RCDs, and the results are shown in Fig. 2(f) and 3(e), where the cell survival rate was above 95% and the average survival rate of bacteria was greater than 91% for EDTA–Zn concentrations in the range of 0–600 μg ml^{-1}, indicating that EDTA–Zn has little toxicity and no bactericidal effect as well as photocatalytic oxidation activity. It is proved once again that EDTA binds to free zinc ions but not to zinc ions doped on the surface of RCDs. From the above, we can conclude that EDTA–Zn-RCDs is a substance with low cytotoxicity and high bactericidal effect, presumably a mixture of EDTA–Zn and Zn-doped carbon dots, while the Zn-doped carbon dots without free zinc ion is what we need for a drug with high catalytic oxidation performance and excellent biocompatibility. We thus propose for the first time a novel method for the construction of highly efficient and low-toxicity photocatalytic carbon nanodots, with the first step consisting in doping with metal ions, the second step involving complexation of the free metal with EDTA and retaining the surface doped metal-carbon dots, which gives rise to a novel thinking and method for the subsequent construction of highly efficient and low-toxicity metal-doped carbon dots. As depicted in Fig. S7,† with the increase in the concentration of EDTA–Zn-RCDs, the average survival rate of *Escherichia coli*

shows a decreasing trend, and when the concentration reaches 600 μg ml^{-1}, the average survival rate reaches 25.9% and the average sterilization rate reaches 74.1%, indicating that this antibacterial strategy also has a significant bactericidal effect on Gram-negative bacteria.

Quantitative test of $^1O_2$ *in vitro*

As depicted in Fig. S5,† the yield of singlet oxygen of RCDs, Zn-RCDs, EDTA–Zn-RCDs, and PpIX with the same concentration outside the cell after blue light stimulation was in the order: Zn-RCDs > EDTA–Zn-RCDs > PpIX > RCDs. Compared with the common high-efficiency photosensitizer PpIX, Zn-RCDs and EDTA–Zn-RCDs produce more singlet oxygen, and according to the one-way ANOVA analysis, there was a significant difference, respectively ($P < 0.0001$, $P < 0.0001$). It can be seen that doping zinc can significantly improve the photocatalytic efficiency of carbon dots and greatly improve their optical properties. The singlet oxygen yield of EDTA–Zn-RCDs decreased slightly compared with the Zn-RCDs, because it contains EDTA–Zn, which reduces the content of zinc-doped carbon dots.

Quantitative test of ROS

As depicted in Fig. S6(a),† in cells with the same concentration of RCDs, Zn-RCDs, EDTA–Zn-RCDs and PpIX, after receiving blue light stimulation, the production of reactive oxygen species followed the order: Zn-RCDs > EDTA–Zn-RCDs > PpIX > RCDs. Compared with the common high-efficiency photosensitizer PpIX, Zn-RCDs and EDTA–Zn-RCDs produce more reactive oxygen species, and according to the one-way ANOVA analysis, there was a significant difference, respectively ($P < 0.0001$, $P < 0.0001$). It can be seen that doping zinc can significantly improve the photocatalytic efficiency of carbon dots and greatly improve their optical properties. Compared with Zn-RCDs, the reactive oxygen species production of EDTA–Zn-RCDs decreased slightly, because it contains EDTA–Zn, resulting in the decrease of the content of zinc-doped carbon dots. It is consistent with the results of the quantitative test of singlet oxygen *in vitro* and with the results of the bactericidal effect experiment presented in Fig. S6(b).† Compared with the common high-efficiency photosensitizer PpIX, Zn-RCDs and EDTA–Zn-RCDs have lower *S. aureus* viability, and according to one-way ANOVA analysis, there was a significant difference, respectively ($P < 0.0001$, $P < 0.0001$).

Validation experiment of the bactericidal mechanism and the ROS staining assay

Validation experiment of the bactericidal mechanism. As depicted in Fig. 3(g), the fluorescence intensity of DCFDA increased with increasing concentrations of EDTA–Zn-RCDs and corresponded to the decrease in bacterial survival with increasing concentrations of EDTA–Zn-RCDs in Fig. 3(f), thus indicating that with increasing concentrations of EDTA–Zn-RCDs, the production of reactive oxygen species increased, leading to a decrease in bacterial survival and an increase in bactericidal rate. This also demonstrates the intrinsic mechanism of the bactericidal activity of EDTA–Zn-RCDs.

ROS staining experiment. As depicted in Fig. 4, under fluorescence microscopy, the control, blue light, and EDTA–Zn-RCD groups could all be observed under a bright field as grape-like *S. aureus* with a near-transparent cell edge layer and a grey interior, a standard *S. aureus* morphology with a regular shape and uniform size, while none of these three groups show obvious green fluorescence under dark field, and it could be inferred that there was no production of reactive oxygen species, while in the case of the EDTA–Zn-RCDs + blue light group, observed under the bright field, the morphology of *S. aureus* became irregular and uneven in size, and larger than normal *S. aureus cells*. When observed under the dark field, there was obvious green fluorescence, thus suggesting that EDTA–Zn-RCDs and blue light irradiation alone did not produce reactive oxygen species or kill the bacteria. In contrast, the new bactericidal strategy of EDTA–Zn-RCDs + blue light produced an abundance of ROS and had a significant bactericidal effect on *Staphylococcus aureus*.

Live and dead bacteria staining experiments

As depicted in Fig. 5, under the fluorescence microscope, grape-like *S. aureus* could be observed in the control, blue light, and EDTA–Zn-RCD groups under a bright field, with the edge layer of the cells being nearly transparent and the interior appearing grey, a standard *S. aureus* morphology with a more regular shape and more uniform size, but the *S. aureus* in the EDTA–Zn-RCD group was larger than that in the control and blue light groups and the bacteria were somewhat larger, and also larger in comparison to Fig. 4, presumably because the ROS staining was observed by fluorescence microscopy immediately after drug treatment, whereas PI staining was observed after 24 h, especially in the groups with added drugs such as the EDTA–Zn-RCD group and the EDTA–Zn-RCDs + blue light group, presumably during this 24 h, due to the good biocompatibility of zinc-doped carbon dots. With time, the more carbon dots entered the cells, the larger the cells appeared. At the same time,

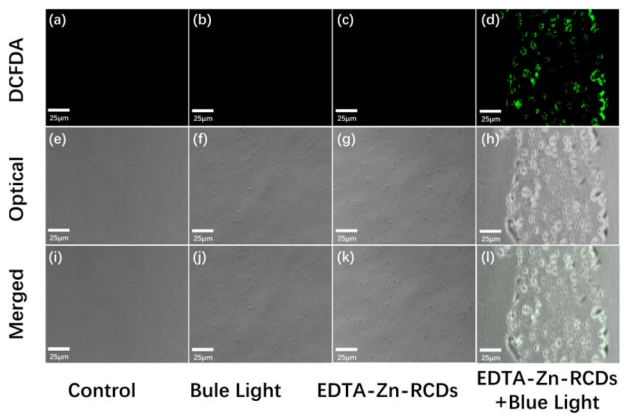

Fig. 4 The effect of EDTA–Zn-RCDs and blue light upon intracellular ROS generation in *S. aureus* was assessed by DCFDA staining immediately after the subsequent treatments. (a), (e) and (i) Control; (b), (f) and (j) blue light alone; (c), (g) and (k) EDTA–Zn-RCDs alone and (d), (h) and (l) EDTA–Zn-RCDs and blue light. ($n = 3$.)

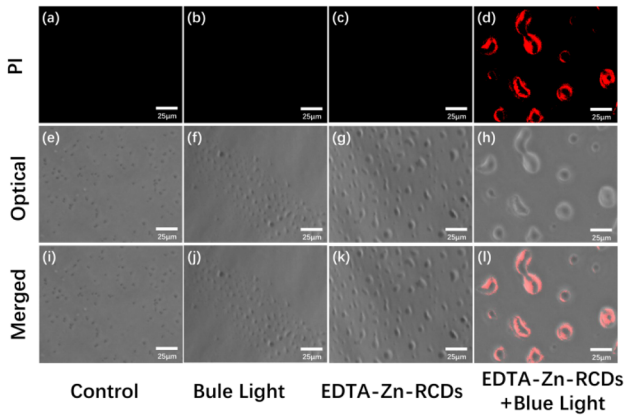

Fig. 5 The role of EDTA–Zn-RCDs and blue light in damaging *S. aureus* was assessed by PI staining at 24 h after the subsequent treatments. (a), (e) and (i) Control; (b), (f) and (j) blue light alone; (c), (g) and (k) EDTA–Zn-RCDs alone and (d), (h) and (l) EDTA–Zn-RCDs and blue light. ($n = 3$).

no obvious red fluorescence was seen in any of these three groups under a dark field, which indicates that no dead cells were produced, and further proves the good biocompatibility of the Zn-doped carbon dots. In contrast, in the EDTA–Zn-RCDs + blue light group, the morphology of *S. aureus* became irregular and uneven in size and much larger than normal *S. aureus* cells when observed under a bright field, and there was obvious red fluorescence when observed under a dark field, thus suggesting that EDTA–Zn-RCDs and blue light irradiation alone did not kill the bacteria, while the new bactericidal strategy of EDTA–Zn-RCDs + blue light would kill the bacteria and had a significant bactericidal effect on *Staphylococcus aureus*.

Bacterial plate assay

We used the bacterial plate coating method to explore the antibacterial effect of EDTA–Zn-RCDs + blue light more visually, as depicted in Fig. 6. For the blue light alone and EDTA–Zn-RCD groups alone, compared with the control group, there was no obvious change in the number of bacteria on the plates, while for the EDTA–Zn-RCDs + blue light group, only a few colonies grew on the plates, once again demonstrating the strong antibacterial effect of EDTA–Zn-RCDs + blue light. The synergistic treatment showed a strong antimicrobial effect, which corroborated with the results measured quantitatively using the microplate reader, and again demonstrated the good biosafety of blue light and EDTA–Zn-RCDs alone, and we could visually localize the lesion or direct the light to the lesion by imaging, laying the foundation for subsequent *in vivo* local mouse wound model studies.

Drug resistance assay

To examine whether our antibacterial regimen can break through the infection of drug-resistant bacteria, we simulated the bacterial resistance process and repeated the experiment for 7 rounds. After each round, the surviving *S. aureus* were isolated immediately after the survival rate measurement and subjected to the relevant treatment in the next round, the results are shown in Fig. 7. The average bacterial survival rate for the 7 times were 10.32%, 10.07%, 10.17%, 9.86%, 9.85%, 9.46% and 10.35%, which indicate that our new antibacterial protocol EDTA–Zn-RCDs + blue light does not allow bacteria to develop resistance, has the advantages of low drug resistance, minimal marginal tissue damage and low toxic side effects, and has great potential for clinical translation for the treatment of drug-resistant bacterial infections.

In vivo antimicrobial assay

Fig. S8† depicts the flow chart of the animal model treatment. The model is carried out on day 0, treatment is carried out on day 2, and wound pictures are collected at different time points (0, 2, 4, 6, 8, and 10 d). On the 10th day, the mice were killed for bacterial reverse culture, tissue embedding, sectioning, and staining.

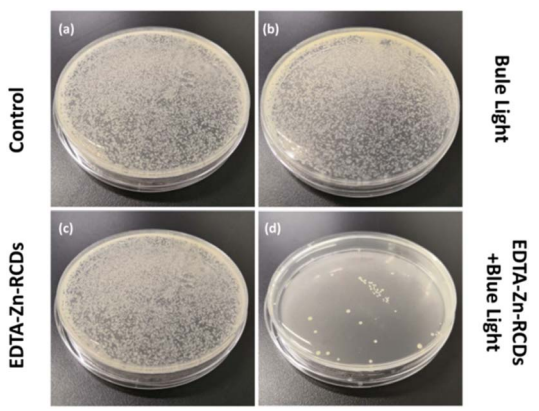

Fig. 6 The role of EDTA–Zn-RCDs and blue light in damaging *S. aureus* was revealed by the single *S. aureus* colony on an LB plate. (a) Control; (b) blue light alone; (c) EDTA–Zn-RCDs alone and (d) EDTA–Zn-RCDs and blue light. ($n = 3$.)

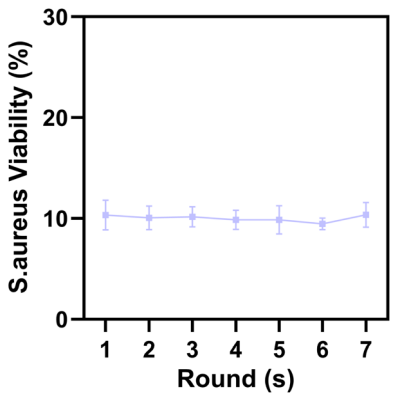

Fig. 7 The *in vitro* sustained anti-bacterial effect was assessed by recording the viability of *S. aureus* at 24 h after 7 rounds of treatment with the EDTA–Zn-RCDs and blue light. Following each round, surviving *S. aureus* were immediately isolated after viability measurement and subjected to the relevant treatment in the next round ($n = 6$).

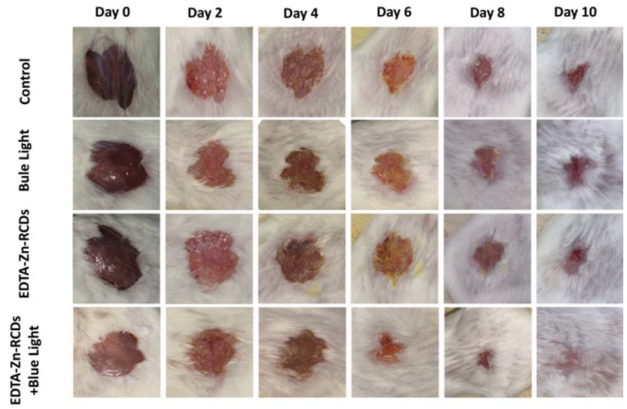

Fig. 8 Pictures of wounds of four groups of infected mice at different time points ($n = 6$).

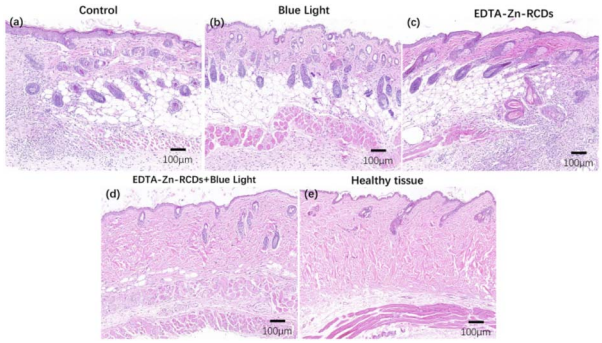

Fig. 9 H&E chromatogram of infected skin tissues from different treatment groups (a) control; (b) blue light alone; (c) EDTA–Zn-RCDs alone and (d) EDTA–Zn-RCDs and blue light; (e) healthy tissue. ($n = 6$.)

For the sake of better visual monitoring of the effect of different treatment regimens on the wounds of mice, we collected wound pictures at 0 d, 2 d, 4 d, 6 d, 8 d, and 10 d, respectively, as depicted in Fig. 8, for four groups of animals: control group, EDTA–Zn-RCD group, blue light group, and EDTA–Zn-RCDs + blue light group. With time, the wounds of all four groups tended to gradually become smaller. And in the EDTA–Zn-RCDs and blue light groups, the wounds did not become smaller or heal significantly compared with the control group, whereas in the EDTA–Zn-RCDs + blue light group, the wounds became smaller compared to the control group, and all wounds had healed by day 10, and the formation of new skin tissue was visible in the graph.

We also took the skin of mice at the wound site on day 10 for bacterial counter-culture to observe the number of bacteria in their wounds. As depicted in Fig. S9,† for five groups of animals: control, EDTA–Zn-RCDs, blue light, EDTA–Zn-RCDs + blue light, and healthy group, the number of bacterial colonies in the animals in the EDTA–Zn-RCDs and blue light groups did not decrease significantly compared to the control group. This indicates that EDTA–Zn-RCDs alone and blue light irradiation alone had no inhibitory effect on bacteria, while the EDTA–Zn-RCDs + blue light group showed a significant decline in the amounts of bacterial colonies, compared with the control group and it was comparable to that of the healthy group, indicating that the new antibacterial strategy of EDTA–Zn-RCDs + blue light still has good bactericidal effects on bacterial infections in the wounds of mice *in vivo*. According to the one-way ANOVA analysis, there was a significant difference, respectively ($P < 0.0001$). A graph of their corresponding bacterial survival statistics is shown in Fig. S10.† The bacterial survival rate of the EDTA–Zn-RCDs + blue light group was remarkably different from that of the control group and similar to that of the healthy group, with an average bacterial survival rate of 8.83% and an average bactericidal efficiency of 91.17%.

Meanwhile, we executed mice on day 10 and removed their heart, liver, spleen, lung, kidney, and skin for embedding, sectioning, and HE staining, as depicted in Fig. 9. Histological analysis of the infected skin of the five groups of animals was performed: control, EDTA–Zn-RCDs, blue light, EDTA–Zn-RCDs + blue light, and healthy group. The number of inflammatory cells (blue cells) in the animals with the EDTA–Zn-RCD group alone and blue light alone groups was not significantly low compared with the control group, and many denser inflammatory cells could still be observed, whereas the number of inflammatory cells remarkably declined in the EDTA–Zn-RCDs + blue light group compared to the control group, but some more sparsely scattered inflammatory cells could still be observed, similar to the number of inflammatory cells in the healthy group, which could also indicate that the EDTA–Zn-RCDs + blue light treatment regimen was effective in relieving inflammation at the infection site at day 10. We also collected the organs (heart, liver, spleen, lungs, and kidneys) of each mouse on day 10 and performed histological analysis of organ sections from the five groups of animals: control group, EDTA–Zn-RCDs group, blue light group, EDTA–Zn-RCDs + blue light group and healthy group to examine the toxic effects of EDTA–Zn-RCDs in mice, as depicted in Fig. S11,† and found that there was no significant visceral damage in any of the groups or inflammatory injury, and there was no remarkable difference between these groups, indicating that the toxicity of EDTA–Zn-RCDs in mice was minimal and the biosafety was good.

Conclusions

This project proposes a highly effective photosensitizer that breaks through drug-resistant bacterial infections with zinc-doped carbon dots. By passing through the membrane of drug-resistant bacteria, the photosensitizer produces ROS in bacteria under the action of blue light power to directly kill bacteria, so as to realize the antibacterial local treatment of drug-resistant bacteria and its traumatic infection model.

The study has the following advantages over the current bactericidal treatment protocols reported in the literature as depicted in Table S1.† Firstly, the method involves the use of an efficient and economical one-step hydrothermal approach for the preparation of zinc-doped red-light CDs as a photosensitizer, doping zinc metal as a photooxidation catalyst into the carbon dots. Secondly, the raw materials are economical and easily available. Thirdly, it has both low cytotoxicity and good biocompatibility. Fourthly, it also maintains the catalytic

oxidation performance of zinc metal and greatly improves the sterilization rate and the efficiency of ROS generation, which is higher than that of PpIX. In addition, it provides a convenient idea and method for researchers to prepare highly efficient and low-toxicity metal-doped carbon dots, which can be subsequently prepared using other metals and then attenuated using EDTA to use this method in the treatment of other diseases like cancer. What's more, it was then verified through bactericidal effect experiments and *in vivo* animal experiments that this antibacterial method has great potential for clinical translation. The bactericidal efficiency of this antibacterial regimen against *S. aureus* was as high as 90%. And further studies in a mouse model showed that this treatment regimen showed effective antibacterial activity, requiring only one complete treatment to show a significant difference with a bactericidal effect of 91.17%. More notably, after seven repeated treatments simulating the bacterial resistance process, the bactericidal efficiency was still 90%, showing that our method has the potential to break through drug-resistant bacterial infections as an alternative antibiotic candidate as well as one of the treatment options.

However, as the lyophilized re-solvated samples showed large clusters of material under transmission electron microscopy but not in the un-lyophilized stock solution, we have only used this antimicrobial solution in a localized *in vivo* model to prevent vascular obstruction and to improve the safety of animal experiments. Subsequent explorations can be continued based on the stock solution. It is hoped that this stock solution can be used in a systemic model, not just *in vitro*, to provide an alternative to antibiotics in the treatment of deep-seated tissues and organs, especially in the treatment of drug-resistant osteomyelitis and peritonitis.

Conflicts of interest

There are no conflicts to declare.

Acknowledgements

Sichuan Key Research and Development Project of China (2020YFS0260) provided funds for this program. The authors are always grateful for the financial support offered by the Department of Science and Technology of Sichuan Province.

References

1 D. Pornpattananangkul, L. Zhang, S. Olson, S. Aryal, M. Obonyo, K. Vecchio, C. M. Huang and L. Zhang, *J. Am. Chem. Soc.*, 2011, **133**, 4132–4139.
2 G. Taubes, *Science*, 2008, **321**, 356–361.
3 S. B. Levy and B. Marshall, *Nat. Med.*, 2004, **10**, S122–S129.
4 F. Xu, Y. Zhao, M. Hu, P. Zhang, N. Kong, R. Liu, C. Liu and S. K. Choi, *Chem. Commun.*, 2018, **54**, 9525–9528.
5 T. Maisch, *Mini-Rev. Med. Chem.*, 2009, **9**, 974–983.
6 P. Manivasagan, F. Khan, G. Hoang, S. Mondal, H. Kim, V. Hoang Minh Doan, Y. M. Kim and J. Oh, *Carbohydr. Polym.*, 2019, **225**, 115228.
7 S. Na, J. H. Kim, Y. K. Rhee and S. W. Oh, *Food Sci. Biotechnol.*, 2018, **27**, 203–210.
8 Y. Zhang, P. Sun, L. Zhang, Z. Wang, F. Wang, K. Dong, Z. Liu, J. Ren and X. Qu, *Adv. Funct. Mater.*, 2019, **29**, 1–9.
9 R. R. Allison and K. Moghissi, *Clinical Endoscopy*, 2013, **46**, 24–29.
10 B. Li, L. Lin, H. Lin and B. C. Wilson, *J. Biophotonics*, 2016, **9**, 1314–1325.
11 M. R. Hamblin and T. Hasan, *Photochem. Photobiol. Sci.*, 2004, **3**, 436–450.
12 F. Harris and L. Pierpoint, *Med. Res. Rev.*, 2012, **32**, 1292–1327.
13 H. Neda, K. Farzaneh and B. Abbas, *J. Appl. Oral Sci.*, 2014, **22**, 80–84.
14 J. W. Liou and H. H. Chang, *Arch. Immunol. Ther. Exp.*, 2012, **60**, 267–275.
15 Y. Sun, B. Zhou, Y. Lin and W. Wang, *J. Am. Chem. Soc.*, 2006, **128**, 7756–7757.
16 J. A. Jaleel and K. Pramod, *J. Controlled Release*, 2018, **269**, 302–321.
17 S. Y. Lim, W. Shen and Z. Gao, *Chem. Soc. Rev.*, 2015, **44**, 362–381.
18 P. Miao, K. Han, Y. Tang, B. Wang, T. Lin and W. Cheng, *Nanoscale*, 2015, **7**, 1586–1595.
19 B. Ju, H. Nie, X.-g. Zhang, Q. Chen, X. Guo, Z. Xing, M. Li and S. X.-A. Zhang, *ACS Appl. Nano Mater.*, 2018, **1**, 6131–6138.
20 P. Das, S. Ganguly, M. Bose, S. Mondal, S. Choudhary, S. Gangopadhyay, A. K. Das, S. Banerjee and N. C. Das, *Mater. Sci. Eng., C*, 2018, **88**, 115–129.
21 M. J. Meziani, X. Dong, L. Zhu, L. P. Jones, G. E. LeCroy, F. Yang, S. Wang, P. Wang, Y. Zhao, L. Yang, R. A. Tripp and Y. P. Sun, *ACS Appl. Mater. Interfaces*, 2016, **8**, 10761–10766.
22 A. T. Bell, *Science*, 2003, **299**, 1688–1691.
23 H. Chen, X. He, Z. Zhou, Z. Wu, H. Li, X. Peng, Y. Zhou, C. Tan and J. Shen, *J. Nanobiotechnol.*, 2022, **20**, 136.
24 W. Shen, T. Hu, X. Liu, J. Zha, F. Meng, Z. Wu, Z. Cui, Y. Yang, H. Li, Q. Zhang, L. Gu, R. Liang and C. Tan, *Nat. Commun.*, 2022, **13**, 3384.
25 Z. Zhou, Y. Wang, F. Peng, F. Meng, J. Zha, L. Ma, Y. Du, N. Peng, L. Ma, Q. Zhang, L. Gu, W. Yin, Z. Gu and C. Tan, *Angew. Chem., Int. Ed. Engl.*, 2022, **61**, e202115939.
26 Y. Yamada, T. Miyahigashi, H. Kotani, K. Ohkubo and S. Fukuzumi, *J. Am. Chem. Soc.*, 2011, **133**, 16136–16145.
27 C. Ding, A. Zhu and Y. Tian, *Acc. Chem. Res.*, 2014, **47**, 20–30.
28 L. Cao, M. Meiani, S. Sahu and Y. Sun, *Acc. Chem. Res.*, 2013, **46**, 7–17.
29 H. Li, Z. Kang, Y. Liu and S.-T. Lee, *J. Mater. Chem.*, 2012, **22**, 24175–24478.
30 X. Li, S. Zhang, S. A. Kulinich, Y. Liu and H. Zeng, *Sci. Rep.*, 2014, **4**, 1–8.
31 Q. Liu, B. Guo, Z. Rao, B. Zhang and J. R. Gong, *Nano Lett.*, 2013, **13**, 2436–2441.
32 M. Wu, Y. Wang, W. Wu, C. Hu, X. Wang, J. Zheng, Z. Li, B. Jiang and J. Qiu, *Carbon*, 2014, **78**, 480–489.

33 H. Li, R. Liu, Y. Liu, H. Huang, H. Yu, H. Ming, S. Lian, S.-T. Lee and Z. Kang, *J. Mater. Chem.*, 2012, **22**, 17351–18064.
34 X. Zhang, F. Wang, H. Huang, H. Li, X. Han, Y. Liu and Z. Kang, *Nanoscale*, 2013, **5**, 2274–2278.
35 F. Wang, M. Kreiter, B. He, S. Pang and C. Y. Liu, *Chem. Commun.*, 2010, **46**, 3309–3311.
36 S. Chandra, P. Patra, S. H. Pathan, S. Roy, S. Mitra, A. Layek, R. Bhar, P. Pramanik and A. Goswami, *J. Mater. Chem. B*, 2013, **1**, 2375–2382.
37 X. Li, Y. Liu, X. Song, H. Wang, H. Gu and H. Zeng, *Angew. Chem., Int. Ed. Engl.*, 2015, **54**, 1759–1764.
38 J. Ge, M. Lan, B. Zhou, W. Liu, L. Guo, H. Wang, Q. Jia, G. Niu, X. Huang, H. Zhou, X. Meng, P. Wang, C. S. Lee, W. Zhang and X. Han, *Nat. Commun.*, 2014, **5**, 4596.
39 Y. Yang, J. Zhang, X. Wu, Y. Fu, H. Wu and S. Guo, *J. Mater. Chem. A*, 2014, **2**, 9111–9117.
40 Z. Qian, X. Shan, L. Chai, J. Ma, J. Chen and H. Feng, *ACS Appl. Mater. Interfaces*, 2014, **6**, 6797–6805.
41 D. Sun, R. Ban, P.-H. Zhang, G.-H. Wu, J.-R. Zhang and J.-J. Zhu, *Carbon*, 2013, **64**, 424–434.
42 J. P. Paraknowitsch, Y. Zhang, B. Wienert and A. Thomas, *Chem. Commun.*, 2013, **49**, 1208–1210.
43 W. Wu, L. Zhan, W. Fan, J. Song, X. Li, Z. Li, R. Wang, J. Zhang, J. Zheng, M. Wu and H. Zeng, *Angew. Chem., Int. Ed. Engl.*, 2015, **54**, 6540–6544.
44 S. Xue, T. Zhang, X. Wang, Q. Zhang, S. Huang, L. Zhang, L. Zhang, W. Zhu, Y. Wang, M. Wu, Q. Zhao, P. Li and W. Wu, *Small*, 2021, **17**, e2102178.
45 D. Y. Guo, C. X. Shan, S. N. Qu and D. Z. Shen, *Sci. Rep.*, 2014, **4**, 7469.
46 Y. Li, B.-P. Zhang, J.-X. Zhao, Z.-H. Ge, X.-K. Zhao and L. Zou, *Appl. Surf. Sci.*, 2013, **279**, 367–373.
47 Y. Cai, C. Cao, X. He, C. Yang, L. Tian, R. Zhu and Y. Pan, *Nanomedicine*, 2016, **12**, 505–506.
48 Z. M. Markovic, B. Z. Ristic, K. M. Arsikin, D. G. Klisic, L. M. Harhaji-Trajkovic, B. M. Todorovic-Markovic, D. P. Kepic, T. K. Kravic-Stevovic, S. P. Jovanovic, M. M. Milenkovic, D. D. Milivojevic, V. Z. Bumbasirevic, M. D. Dramicanin and V. S. Trajkovic, *Biomaterials*, 2012, **33**, 7084–7092.
49 X. Zhao, Q. Tang, S. Zhu, W. Bu, M. Yang, X. Liu, Y. Meng, W. Yu, H. Sun and B. Yang, *Nanoscale*, 2019, **11**, 9526–9532.
50 Z. Zhong, X. Li, S. Liu, C. Zhang, X. Xu and L. Liao, *RSC Adv.*, 2021, **11**, 28809–28817.